



# Optimization of a Single-Phase Induction Motor Using Finite Element Method

*Ikeagu Nnamdi Michael and Prof. I. I. Eneh*

Enugu State University of Science and Technology

[nnamdiikeagu77@gmail.com](mailto:nnamdiikeagu77@gmail.com)

DOI : <https://doi.org/10.55248/gengpi.6.0225.1020>

## ABSTRACT

This study applies Finite Element Method (FEM) to optimize the speed of 3<sup>rd</sup> harmonic of Single-Phase Induction Motor (SPIM). This work is focused on current, torque, efficiency, and losses of the SPIM using experimental and simulation-based methods. The study shows how motor behaviour, harmonic distortions, and increasing speed interact. The third harmonic content increases from 0% to 18% as the motor speed climbs from 0 to 1800 rpm. Because there is less slide, the current draw drops dramatically from 25A to 5.21A, indicating improved electrical efficiency at higher speeds. An ideal operating range at mid-level speeds is indicated by the torque, which peaks at 12.985 Nm at 1400 rpm and then decreases to 0.527 Nm at 1800 rpm. With significant peaks at 1400 rpm (67.96%) and 1600 rpm (70.87%), efficiency increases from 58.88% at 0 rpm to a maximum of 72.94% at 1800 rpm. As speed increases, mechanical losses grow from 0W to 188.52W because of windage and friction, but copper losses substantially reduce from 312.5W to 13.5721W. The overall losses exhibit a complicated pattern, decreasing around 1600 rpm and then marginally increasing at higher speeds. At higher speeds, the SPIM achieves increased efficiency despite the rise in mechanical losses and harmonic content. These results highlight how crucial it is to optimize motor design and control schemes in order to minimize the effects of harmonic distortions and balance efficiency, torque, and losses.

**Keywords:** Single-Phase Induction Motor (SPIM); Induction Machine; Harmonic Distortion; Motor Efficiency; Torque Characteristics; Copper Losses

## 1. INTRODUCTION

Getting the best out of the performance of electrical machines has remained a center of research attention for many decades now. This is because electrical machines have remained the heart of many mechanical and electrical designs: a prime mover to facilitate the drive of other mechanisms in engineering settings. According to Mircea et al. (2014), the most used industrial machine is induction motor, due to the low cost and high reliability. Induction motors are electrical motors which operates using rotor current to produce torque for the stator winding through the principle of electromagnetic induction (Byung et al., 2006), and are of two major categories which are the squirrel cage and slip ring motor.

Today over 90% of employed induction motors are grouped under the category of squirrel cage rotor type, due to their robust nature, simplicity, robust construction nature, user friendly, affordability, ability to generator torques over variable speed, and ability for self-rotor excitation supply from the stator through electronic magnetic induction process, etc. (Khan et al., 2018; Ghadimi et al., 2011; Singh. 2012; Anih et al., 2015). These induction motor in addition are various types, based on their phases which ranges from single phase, double phase, three phase and others (Hamed and Hamid, 2022).

According to Mohd and Gurmeet (2007), the Single-Phase Induction Motor (SPIM) has dominated the design components for electrical appliances. This SPIM also dominated the category of interconnected load in power system network (Ghadimi et al., 2011). SPIM are of various classification based on ancillary services which are the capacitor start motor, capacitor start and run motor, split-phase motor, permanent split capacitor motor and shaded pole motor (Singh, 2012; Obe, 2007). In recent times, the issue of harmonics has evolved to be a major threat to the optimal performance of SPIM. Harmonics are distorted signal which affects the dynamics of the motor operation and are of two major types which are space and time harmonics (Liang and Luy, 2006). The space type originates from the difference between the phase winding interactions, when sinusoidal power is supplied to the motor (Alexandre et al., 2020), while time harmonics originated from the nonlinear behavior of interconnected loads (Singh, 2012; Neto et al., 2018).

All these forms of harmonics have impact on the quality of motor performance, but the time harmonics can be controlled by controlling the interconnected load, while the space harmonics on the other hand is more complex to manage (Alexandre et al., 2020) as the source was originated from the air gap, due to poor winding design (Chao and Li, 2022) and results to technical problems such as poor efficiency, unbalanced power factor, losses, high energy consumption, temperature effect of overheating, and torque ripple (Usha et al., 2022); hence presented the need analysis.

In the space harmonics, various odd harmonics such as 3<sup>rd</sup>, 5<sup>th</sup>, 7<sup>th</sup>, 11<sup>th</sup>, etc. impacts on the dynamics of the induction motor modeling and has continue to attract research attention. In addition (Chen et al. 2022; Pereira et al., 2016) posited that 3<sup>rd</sup> harmonics induced from the air gap of induction machines have more impact on the performance of input impedance and overall dynamics of the machine than other types of harmonics.

Over the past four decades, many literatures has flourished the modeling of induction motor, considering harmonics, using various approaches such as (Leonardo et al., 2020; Usha et al., 2022; Chen et al., 2022) which employed numerical approaches which employed Finite Element Method (FEM) for the analysis and modeling of induction motor. But despite the success (Petro et al., 2011; Alberto et al., 2021) posted that the approach is to complex for implementation by system design engineers, also it is time consuming during processing (Carla et al., 2021). Other method is the dq-0 direct axis algorithm (Lee et al., 2022), which has the capacity to model the behavior of machine and also less complex when compared to FEM, but Carla et al. (2021) posited that solution for the model has not been obtained which considered harmonics. Circuit based method in Huang et al. (2022) was also proposed for modeling induction motor dynamics, considering Multiple Coupled Circuit (MCC) but Carla et al. (2021) argued that the approach do not guarantee modeling accuracy, based on certain assumptions like uniformity in the air gap.

Geometric approach also involved redesign of the winding function as in (Ojaghi et al., 2018; Hamed and Hamid, 2022), but do not also guarantee accuracy of machine modeling. Yu et al. (2022) used adaptive filter to mitigate online current harmonic. Alexander et al. (2020) applied coil pitch reduction approach, and achieved success in mitigating 7<sup>th</sup> order harmonics current, with little impact on 3<sup>rd</sup> harmonics. However, from the study, the numerical approach was singled out as the most effective based on the evidence of accurate modeling of induction motor dynamics.

To this end, this study proposes the modeling of a single-phase induction machine considering 3<sup>rd</sup> harmonic of magneto-motive force. This will be achieved using numeric approach which manages the impact of space harmonics due to air gap from the windings, employing improved differential equations inspired from direct quadrate (d-q) modeling approach for correct representation of the induction motor.

## 2. RESEARCH METHODOLOGY

The methodology used for this research is experimental and simulation methods. In realizing this methodology, first an experiment was performed to investigate the impact of 3<sup>rd</sup> harmonics on SPIM under varying operating condition. The model of the harmonics problem was formulated using data presentation and analysis approach. Upon achieving this, the SPIM was mathematically modelled, considering the 3<sup>rd</sup> harmonic problem. Simulation method was used to analyze the model at varying condition and then results obtained from the simulation were analyzed comparatively.

### 2.1 Data Collection

To perform the model simulation process, data of SPIM with 3<sup>rd</sup> harmonics was collected from machine Laboratory, Akanu Ibiam Federal Polytechnic, Ebonyi State, Nigeria. The experimental setup for the data collection process involves the subsection of the SPIM to 3<sup>rd</sup> harmonic which was introduced every 10minuites by 2% until 18%, as the speed of the motor increases with 200rpm interval.

## 3. TO DEVELOP A PHASE VARIABLE MODEL OF SPIM CONSIDERING 3<sup>RD</sup> HARMONIC MMF USING FINITE ELEMENT METHOD (FEM)

This section explores the use of FEM for the modeling of the SPIM behavior with 3<sup>rd</sup> harmonics. The methodology utilized to achieve this began with the modeling of the motor behavior in motion considering Maxwell equation which considers the moving frames of the motor and then the impact of 3<sup>rd</sup> harmonics on the current density was also analyzed.

### 3.1 Maxwell equation of motion for the SPIM

Motor operation state was considered with respect to the rotor and velocity ( $v$ ) relative to a reference frame  $O(x, y)$  and a local reference frame  $O^i(x^i, y^i)$  which is moving with rotor. During this process, frames of the motor are determined using Maxwell equation which related the Ampere's Law (1), faraday's law (2), Gauss law of electromagnetic (3) and the current density (4) to model the motion behavior of the motor.

$$\nabla * H = J \quad (1)$$

$$\nabla * E = -j\omega B \quad (2)$$

$$\nabla * B = 0 \quad (3)$$

$$J = \begin{Bmatrix} J_0 & in \Omega_n \\ \sigma E & in \Omega_c \end{Bmatrix} \quad (4)$$

The Equation 1 was used to model the behavior of magnetic fields (H) which are generated by electric current density (J) within the induction motor coils according to the law of Ampere, while the Equation 2 describes the variation of magnetic field (B) and its induced impact on electric field (E), where  $j\omega$  presents the complex term of the frequency and  $\omega$  is the angular frequency of the variable field. The Equation 3 indicates zero divergence in the magnetic flux density, since there is no monopole, while the current density modelled in Equation 4 model the current source in different region of the motor. For a non-conductive region  $\Omega_n$   $J = J_0$ , while for a conductive region  $\Omega_c$ ,  $J = \sigma E$ , with the level of conductivity presented as  $\sigma$  and E defines

he electric field. The electromagnetic phenomena which model the motion effects on the motor, is defined by the relationship between the induced magnetic flux density ( $B^i$ ), the electric field, ( $E^i$ ) and the induced magnetic field.

$$B^i = B \quad (5)$$

$$E^i = E + v * B \quad (6)$$

$$H^i = H \quad (7)$$

$$J^i = J \quad (8)$$

The Equation 5 showed that the induced magnetic flux density in the non-stationary frame is the same as the stationary frame. The Equation 6 modeled the induced electric field in the moving using the total stationary electric field (E) and then non induced electric field (B), with (v) given as the velocity of the moving frames. This equation is used model how the E of the moving reference frame is transformed. The Equation 7 and 8 showed that the induced magnetic field and electric field during stationary and non-stationary condition is similar.

### 3.2 Maxwell equation of motion for the SPIM with 3<sup>rd</sup> Harmonics

Overall, the equations in Section 3.1 form the basis for the modeling of the SPIM behavior during motion based on the principle of stationary and non-stationary frames, as essential parameters or the analysis of induction motor behaviour. To determine the current density  $J$ , the induced electric fields and the motion induced term of the  $v * B$  as shown in Equation 9.

$$J = \sigma E^i = \sigma(E + v * B) \quad (9)$$

Where  $v = \omega * r$ ;  $r$  is the position vecto while  $\omega$  is the angular velocity. To introduce the harmonics component on the motor performance, assuming this Harmonics (H) is also a key component of the motor field and magnetic field a shown in the equation 10 and 11 respectively.

$$E = E_1 + E_H \quad (10)$$

$$B = B + B_H \quad (11)$$

Where  $E_1$  is the fundamental electric field component and  $E_H$  is the 3<sup>rd</sup> harmonic component,  $B_1$  is the fundamental magnetic field component,  $B_H$  is the magnetic field with 3<sup>rd</sup> harmonics. The impact of this harmonics on the motor behavior can be defined as a weak form through test function and integration via the application of Maxwell Equation in 12 and 13 respectively.

$$\int_{\Omega} (\nabla \cdot H) \cdot v d\Omega = \int_{\Omega} J \cdot v d\Omega \quad (12)$$

$$\int_{\Omega} (\nabla \cdot E) \cdot \omega d\Omega = - \int_{\Omega} j \omega B \cdot \omega d\Omega \quad (13)$$

To discretize the domain using the FEM into quadrilateral for of two-dimensional element, the Equation 14 and 15 was applied.

$$E = \sum_i N_i E_i \quad (14)$$

$$B = \sum_i N_i B_i \quad (15)$$

Where  $N_i$  is he shape function. To integrate the H component into the FEM model in Equation 2 presents the fundamental component and the component with 3<sup>rd</sup> harmonics as in Equation 16 and 17 respectively.

$$\int_{\Omega} (\nabla \cdot H_1) \cdot v d\Omega = \int_{\Omega} J_1 \cdot v d\Omega \quad (16)$$

$$\int_{\Omega} (\nabla \cdot H_3) \cdot v d\Omega = \int_{\Omega} J_3 \cdot v d\Omega \quad (17)$$

Overall, the FEM used for the modeling of the SPIM with 3<sup>rd</sup> harmonics adapted Maxwell equation taking into account harmonics components of the motor electric and magnetic fields respectively in Equation 9 and 10, then the formulation of the weak forms in Equation 11 and equation 12. The Equation 9 was discretized as equation 13, while equation 1 was discretize as equation 14. Finally, the Equation 15 and 16 presents the model of the SPIM with 3<sup>rd</sup> harmonics with FEM. To measure the Torque, the relationship between the magnetic flux, magnetic fields, discretized volume and current density was applied in Equation 18;

$$T = \int v^{r*} (j * b) dV \quad (18)$$

### 3.3 The stepwise analysis of the Induction motor with FEM

1. The step wise which showed the analysis of the SPIM with FEM software was presented below;
2. Mesh Definition: this defines the domain of the motor using a square mesh
3. Space definition with harmonics: This defines the FEM spaces with harmonics in the electric field
4. Materials properties: Defines the material conductance and angular frequency with 3<sup>rd</sup> harmonics

5. Weak formulation: The weak form of the motor are defined with fundamental and 3<sup>rd</sup> harmonics
6. Solution: This involves the optimization of the model to show the impact of 3<sup>rd</sup> harmonics of the motor.

The figure 1 presents the flow chart of the SPIM with 3<sup>rd</sup> harmonics MMF using finite element method.

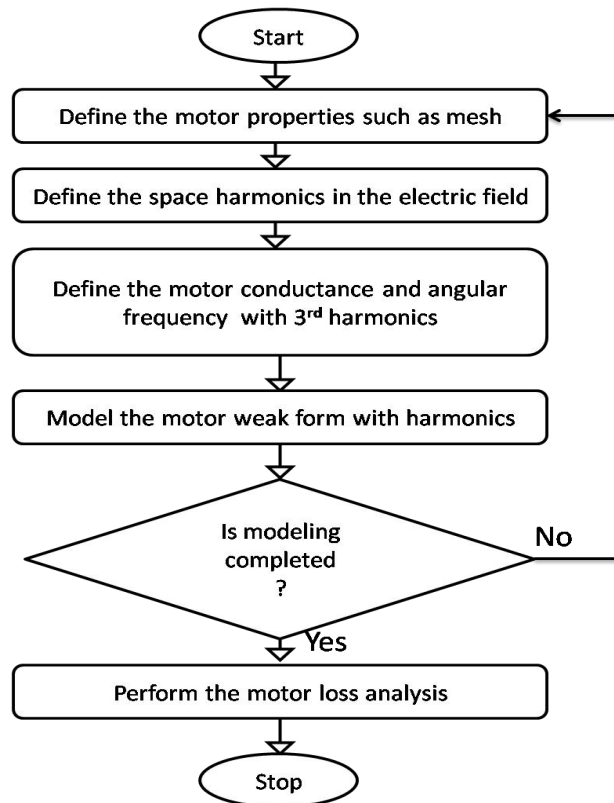


Figure 1: Flowchart of the SPIM with 3<sup>rd</sup> harmonic using finite element method

#### 4. IMPLEMENTATION OF THE SPIM WITH 3<sup>RD</sup> HARMONIC USING FINITE ELEMENT SOFTWARE

The system implementation was done using Finite Element Analysis (FEA) software and online Motor analysis software. The FEA software was used to model the motor behavior with 3<sup>rd</sup> harmonic using finite element method.

##### 4.1 FEA Software for Motor Behavior with Finite Element Method

The FEA software was used to describe the motor activity with third harmonics using the FEM. FEM is a strong numerical technique for solving complicated physical problems. It works by breaking down the entire domain into smaller, simpler sections called finite elements. In the context of motor activity, this entails building a mesh that represents the motor's geometry and calculating the electromagnetic field equations for each element.

The introduction of third harmonics into the motor model entails modifying the electrical inputs to the motor to accommodate these harmonics. This patch enables the software to model the effects of harmonics on motor performance. The FEM method estimates the magnetic flux distribution, eddy currents, and other electromagnetic properties with great precision, taking into account the nonlinear properties of the motor materials as well as the effects of harmonics. The iterative method guarantees that the interactions between magnetic fields and motor components are appropriately represented. The simulation findings assist in identifying spots where harmonics may cause inefficiencies or malfunctions. This information is critical for optimizing the motor design, enhancing performance, and ensuring that it meets operating requirements. The finite element method, used with modern FEA software, enables a thorough and precise analysis of motor behavior in the presence of harmonics, allowing for more effective design and troubleshooting.

#### 5. RESULTS OF SPIM WITH 3<sup>RD</sup> HARMONIC MMF CONSIDERING FEM

This section presents the result of the SPIM simulated with harmonics in FEA software. The discretization of the geometry for the motor designed was presented in the Figure 2.

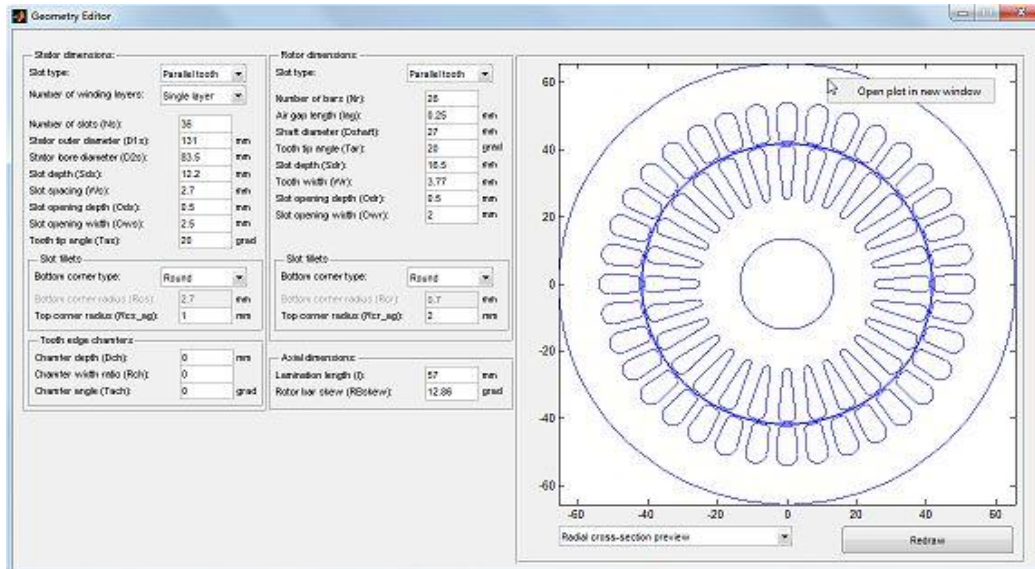


Figure 2: Geometry of the SPIM

Figure 2 presented the modeling of the SPIM considering necessary geometrical inputs for the section to present a radial cross-sectional view of the motor. The model includes the primary motor components such as the stator, air gap, rotor and windings. The stator was configured with the number of slots to house the windings, while the rotor also shows its slot, shaft and windings. The air gap which is between the stator and rotor is also clearly represented, emphasizing its critical role in the motor's magnetic flux path. To generate a finite element period mesh of the motor, the Figure 3 was applied to visualize it.

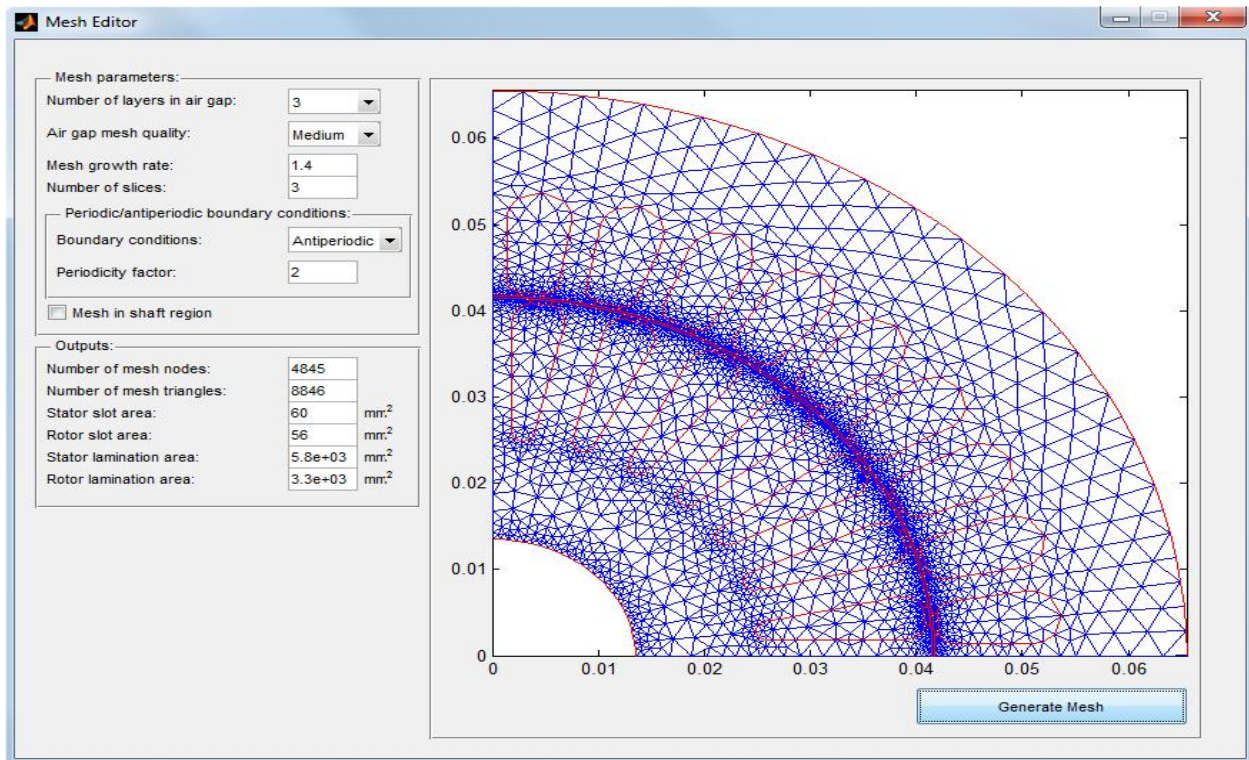


Figure 3: Mesh visualization of the SPIM

Figure 3 illustrates the mesh visualization of the SPIM configuration, highlighting the discretize geometry used in finite element analysis FEA. The stator, rotor, and windings, among other motor components, are all accurately depicted in the mesh. Mesh refinement around critical locations such as the air gap and winding slots ensures more precision in capturing the electromagnetic and thermal distributions. The color coding represents the current density of the windings. The winding properties configuration in the FEA software was presented in the Figure 4;

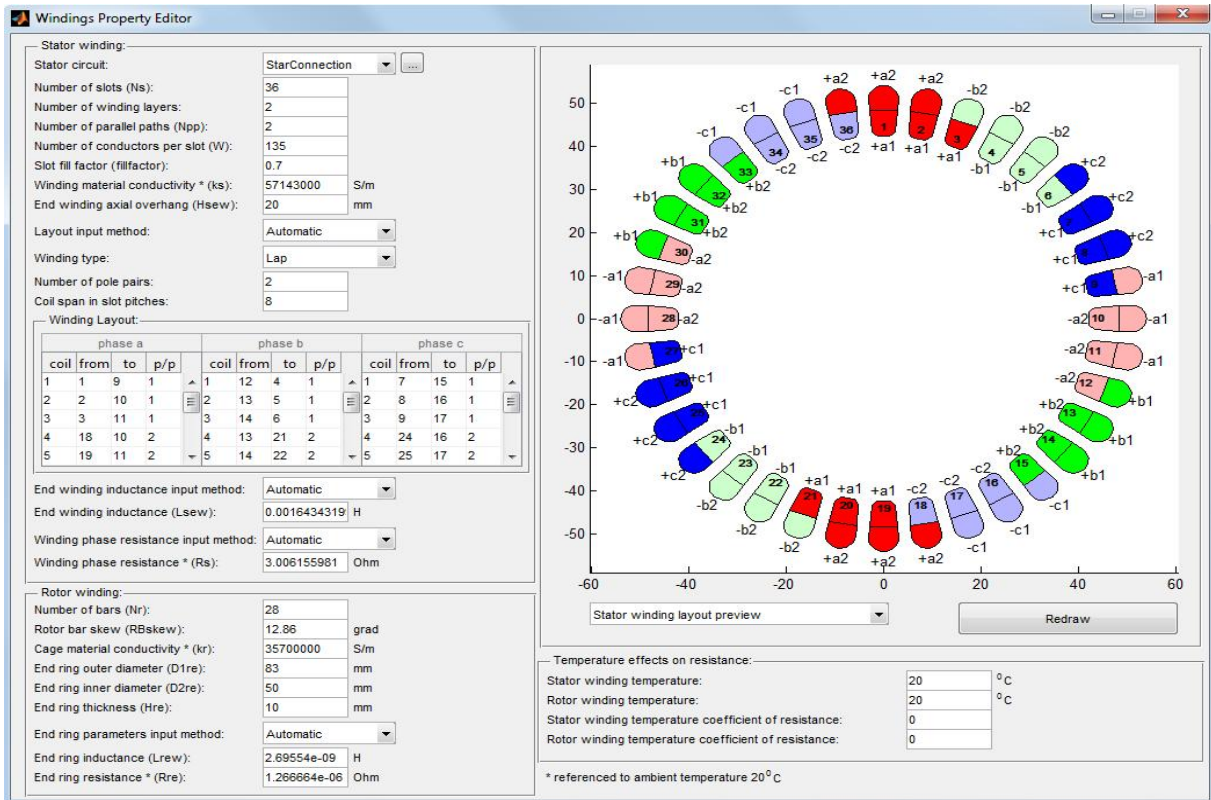


Figure 4: Winding properties of the SPIM

Figure 4 showcased the winding properties of the SPIM, showing the section where detailed specifications of the stator windings such as the winding patterns, number of turns, wire gauge, are configured. This detailed representation is crucial for understanding the electrical characteristics and performance of the motor, providing insights into the efficiency, starting torque, and overall behavior of the SPIM. The figure also showcased the distribution of windings in the stator slots, and their interconnection to form the main and auxiliary windings necessary for the operation of the motor. These properties such as the winding resistance, inductance, and their effect on the magnetic field distribution are depicted in Figure 5 considering Magneto-Motive Force (MMF) third harmonics.

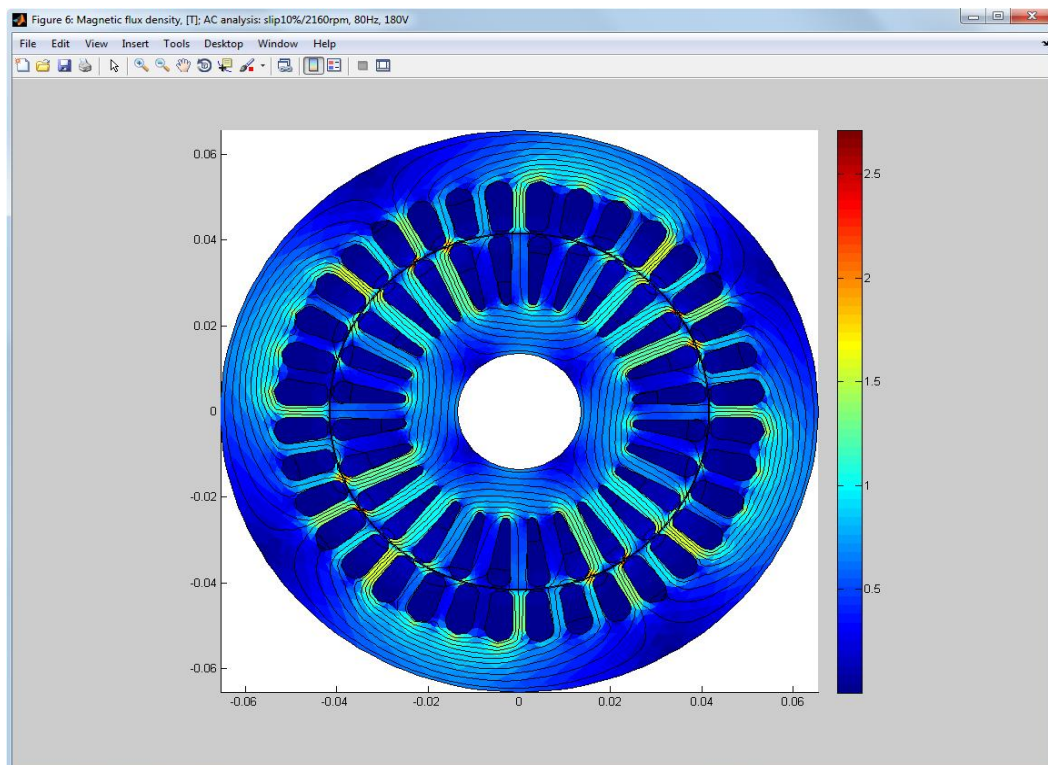


Figure 5: Magnetic field density of the motor with 3<sup>rd</sup> harmonics

Figure 5 presented the distribution of magnetic field with 3<sup>rd</sup> MMF across the motor windings using Maxwell equation, while the electric field distribution was reported. This equation showed the distribution of B across different position of the windings and slots during the motor operation. The model captures the complex interaction of the magnetic field distribution on the motor with MMF 3<sup>rd</sup> harmonics. The color showcased the magnitude of the flux density with the inclusion of 3<sup>rd</sup> harmonics resulting to a non-uniform distribution of the fields especially in the stator and rotor regions and this can affect the motor performance and efficiency. The relative permeability analysis was also showed in Figure 6.

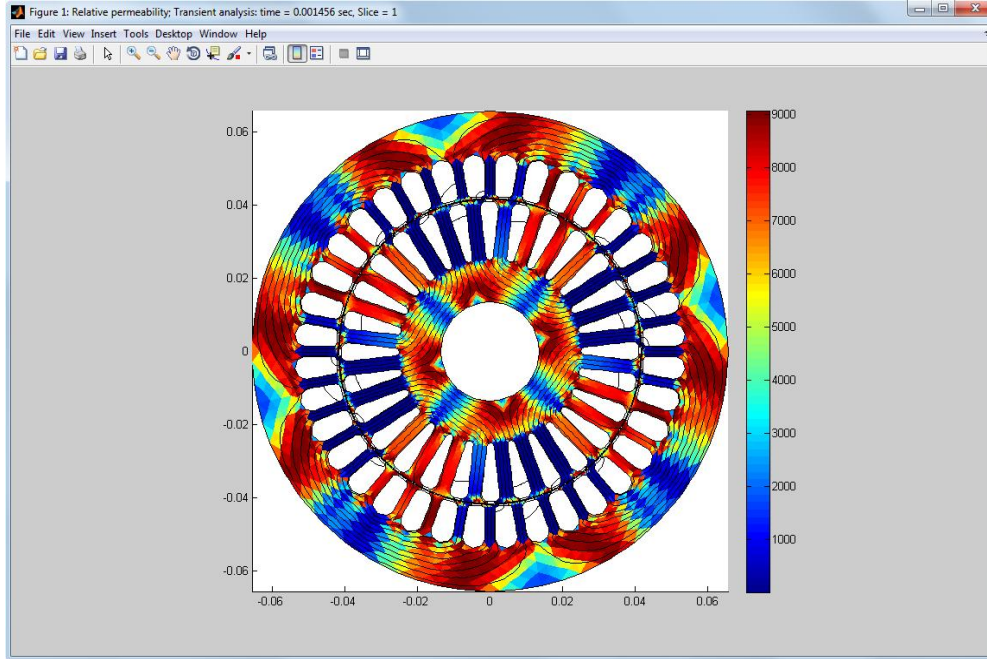


Figure 6: Relative permeability of the SPIM with harmonics

The relative permeability distribution in Figure 6 shows how the motor's permeability fluctuates in the rotor, stator, and air gap. In order to ensure that the model accurately reflects the magnetic properties of the motor, finite elements are used to discretize the model in Equation 11 and 12. Relative permeability values are color-coded, with lower values found in the air gap and greater values often found in the core materials. This help presents a visual model of the distribution of magnetic field on the SPIM with 3<sup>rd</sup> MMF. To measure the current, torque and losses and efficiency on the motor, the Table 1 was applied.

Table 1: Result of SPIM with 3<sup>rd</sup> Harmonics using FEM

| Speed (rpm) | 3 <sup>rd</sup> harmonics (%) | Current (A) | Torque (Nm) | Efficiency (%) | Copper loss (W) | Iron loss (W) | Mechanical loss (W) | Total loss (W) |
|-------------|-------------------------------|-------------|-------------|----------------|-----------------|---------------|---------------------|----------------|
| 0           | 0                             | 25.000      | 0.000       | 58.88158       | 312.5           | 4.32          | 0                   | 312.5          |
| 200         | 2                             | 22.997      | 3.4032      | 62.44453       | 264.431         | 4.32          | 20.9467             | 285.4215       |
| 400         | 4                             | 22.231      | 4.048       | 61.95033       | 247.109         | 4.32          | 41.8933             | 289.1775       |
| 600         | 6                             | 21.844      | 6.203       | 60.28749       | 238.58          | 4.32          | 62.84               | 301.8151       |
| 800         | 8                             | 20.402      | 8.790       | 61.49875       | 208.121         | 4.32          | 83.7867             | 292.6095       |
| 1000        | 10                            | 20.003      | 11.756      | 59.75128       | 200.06          | 4.32          | 104.733             | 305.8902       |
| 1200        | 12                            | 17.981      | 12.001      | 61.98451       | 161.658         | 4.32          | 125.68              | 288.9177       |
| 1400        | 14                            | 13.763      | 12.985      | 67.96228       | 94.7101         | 4.32          | 146.627             | 243.4867       |
| 1600        | 16                            | 10.102      | 10.202      | 70.86755       | 51.0252         | 4.32          | 167.573             | 221.4066       |
| 1800        | 18                            | 5.210       | 0.527       | 72.94131       | 13.5721         | 4.32          | 188.52              | 205.646        |

The effects of speed and third harmonic content on other performance parameters, including as current, torque, efficiency, and losses, are displayed in Table 1. The third harmonic content increases from 0% to 18% as the motor speed increase from 0 to 1800 rpm. The motor's current draw drops from 25 A at 0 rpm to 5.21 A at 1800 rpm, demonstrating better electrical energy efficiency at higher speeds. Induction motors have a general pattern

whereby they consume less current at increasing speeds because of decreased slip. The torque shows the motor's ideal operating range around mid-level speeds; it first rises and peaks at 12.985 Nm at 1400 rpm before falling to 0.527 Nm at 1800 rpm. Efficiency trends reveal interesting insights. The efficiency increases from 58.88% at 0 rpm to a maximum of 72.94% at 1800 rpm, with notable peaks at 1400 rpm (67.96%) and 1600 rpm (70.87%). This suggests that the motor operates most efficiently at higher speeds despite the increased presence of third harmonics, likely due to better electromagnetic coupling and reduced copper losses.

Between 0 rpm and 1800 rpm, copper loss drops dramatically from 312.5 W to 13.5721 W. At higher speeds, there is a corresponding decrease in current draw, which is quite sharp. As should be expected, iron loss is constant at 4.32 W at all speeds since it is mostly influenced by the supply frequency, which stays constant. Mechanical losses rise with increasing rotational speed, from 0W at 0rpm to 188.52W at 1800rpm, due to increased friction and windage losses.

The overall losses show a complicated trend. They first fall, to a minimum of 221.4066 W at 1600 rpm, and then rise slightly to 205.646 W at 1800 rpm. Even with increasing harmonic content and mechanical losses, the SPIM operates more efficiently at higher operating speeds, as seen by the overall decrease in total losses at higher speeds and the improvement in efficiency. The information emphasizes how crucial it is to optimize motor operation and design in order to balance losses, torque output, and efficiency especially when it comes to controlling the effects of harmonic distortions.

---

## 6. CONCLUSION

This study looked into how speed and third harmonic content affected the efficiency, losses, torque, current, and other performance metrics of single-phase induction motors (SPIM). To comprehend the interaction between speed fluctuations and harmonic distortions on motor behaviour, both simulation-based and experimental analyses were carried out. The results highlight important aspects for performance optimisation and offer insightful information about how SPIM operates at different speeds and with third harmonic impacts.

The findings showed that the third harmonic content grew from 0% to 18% as the motor speed climbed from 0 to 1800 rpm. Key performance metrics showed trends suggesting improved motor efficiency at higher speeds despite this increase. From 25 A at 0 rpm to 5.21 A at 1800 rpm, the current draw drastically decreased, following the general pattern of lower current consumption at higher speeds as a result of less slip. The torque peaked at 12.985 Nm at 1400 rpm and then decreased to 0.527 Nm at 1800 rpm, indicating that mid-level speeds would be the ideal operating range. With additional peaks at 1400 rpm (67.96%) and 1600 rpm (70.87%), efficiency significantly increased, peaking at 72.94% at 1800 rpm. These patterns suggest that the motor performs best at higher speeds, most likely as a result of improved electromagnetic coupling and less copper losses.

Additionally, a complex pattern in loss behaviour was discovered by the study. Mechanical losses rose with speed because of windage and friction, going from 0 W at 0 rpm to 188.52 W at 1800 rpm, but copper losses dropped dramatically from 312.5 W at 0 rpm to 13.5721 W at 1800 rpm. Remarkably, total losses decreased at 1600 rpm (221.4066 W) and then increased little at 1800 rpm (205.646 W). The motor's efficiency at higher speeds held up well in spite of these modifications, highlighting the significance of striking a balance between efficiency, torque production, and losses. These results highlight the necessity of sophisticated motor designs and harmonic control techniques to reduce distortions and optimise performance under various operating circumstances.

## REFERENCES

- Alberto, G., Mattia, B., & Emiliano, M. (2021). Critical analysis of FEM modeling procedures for radial bearing stiffness estimation. *Mathematical Problems in Engineering*, 21, Article ID 9955398.
- Anih, L., Obe, S., & Eleanya, M. (2015). Steady state performance of induction and transfer field motor - A comparison. *Nigerian Journal of Technology*, 34(2), 85–391.
- Byung, T., Sung, L., & Byung, K. (2006). Analysis of torque characteristics for single-phase induction motor considering space harmonics. *Journal of Electrical Engineering and Technology*, 1(3), 327–331.
- Carla, T., Javier, M., & Angel, S. (2021). A review of techniques used for the induction machine fault modeling. *MDPI Sensors (Basel)*, 21(14), 4855.
- Chen, H., Zhao, J., Xiong, Y., Yan, S., & Xu, H. (2022). An improved model for five-phase induction motor based on magnetic noise reduction part II: Pole-slot scheme. *Processes*, 10(1430). <https://doi.org/10.3390/pr10081430>
- Correia, A. F. M., Silva, A. M., & Ferreira, F. J. T. E. (2020). Experimental study on the impact of MMF spatial harmonics in the mechanical vibration of a three-phase induction motor. *978-1-7281-9945*, 1560–1568.
- Ghadimi, M., Ramezani, A., & Mohammadimehro, M. (2011). Soft starter modeling for an induction drive starting study in an industrial plant. In *UKSim 5th European Symposium on Computer Modeling and Simulation*. IEEE.
- Hamed, S., & Hamid, R. (2022). A new squirrel cage rotor structure to optimize the dynamic performance of SPIM. *IECO*, ISSN 3517-2645, 281–289.
- Huang, L., Hu, N., Yang, Y., Chen, L., Wen, J., & Shen, G. (2022). Study on electromagnetic–dynamic coupled modeling method—Detection by stator current of the induction motors with bearing faults. *Machines*, 10, 682. <https://doi.org/10.3390/machines10080682>

- Khan, M., Khan, F., Rahman, L., & Fatima, A. (2018). Analysis and electromagnetic noise suppression of three-phase squirrel cage induction motor. In *2018 International Conference on Computing, Electronics and Electrical Engineering (ICE Cube)* (pp. 1–5). IEEE.
- Lee, Y. (2000). Thermal analysis of induction motor with forced cooling channels. *IEEE Transactions on Magnetics*, *36*(4), 1398–1402.
- Leonardo, L., Popescu, M., Tursini, M., Parasiliti, F., & Carbonieri, M. (2020). Transient modeling of induction motors considering space harmonics. *University of L'Aquila UTC from IEEE Xplore*.
- Liang, Y., Qiu, S., Zhang, C., Yang, C., Zhang, J., Yuan, L., & Yang, G. (2021). Equivalent circuit modeling of an induction reaction sphere for micro spacecraft attitude control. *IEEE Transactions on Magnetics*, *57*, 8108108.
- Mircea, P., Claus, B., Miller, T., Malcom, M., & Calum. (2014). Effect of MMF harmonics on single-phase induction motor performance: A unified approach. *IAS Annual Meetings (IEEE Industry and Applications Society)*, 1–8.
- Mohd, A. I., & Gurmeet, S. (2007). A review on influence of rotor geometry on the performance of single-phase capacitor-run induction motor. *International Journal of Advanced Research in Electrical, Electronics and Instrumentation Engineering*, *3*(6), 10216–10224.
- Neto, L., Camacho, J., Salerno, C., & Alvarenga, B. (1999). Analysis of a three-phase induction machine including time and space harmonic effects: The A, B, C reference frame. *Mechanical Engineering from Escola de Engenharia de São Carlos, Universidade de São Paulo (USP)*, São Carlos, Brazil.
- Ojaghi, M., Sabouri, M., & Faiz, J. (2018). Analytic model for induction motors under localized bearing faults. *IEEE Transactions on Energy Conversion*, *33*, 617–626.
- Pereira, L. A., Nicol, G., Pereira, L. F. A., & Skala, B. (2022). Effects of high-order space harmonics on the operation of five-phase induction machines under unbalance. *ISA Transactions*, *131*, 672–692.
- Petro, S., Ihor, F., Piotr, S., & Lukasz, C. (2011). Evaluation of computational complexities of FEM analysis using Gaussian elimination method. *R and I*, *4*, 1–4.
- Singh, G. (2012). Investigation of auxiliary winding harmonic resonance phenomena in single-phase induction motors. *All Theses*, 1561, 1–159. Retrieved from [https://tigerprints.clemson.edu/all\\_theses/1561](https://tigerprints.clemson.edu/all_theses/1561)
- Usha, S., Geetha, A., Thentral, T. M. T., Palanisamy, R., Bajaj, M., Khan, B., & Kamel, S. (2022). Performance investigation of innovative induction motor strategy using magnet for traction application. *International Transactions on Electrical Energy Systems*, 2022, Article ID 7211584, 1–15. <https://doi.org/10.1155/2022/7211584>
- Yu, J., Zhang, Y., Shen, H., & Zheng, X. (2022). Adaptive online extraction method of slot harmonics for multiphase induction motor. *Energies*, *15*, 6643. <https://doi.org/10.3390/en15186643>